Spectral induced polarization: frequency domain versus time domain laboratory data

Martin, Tina; Titov, Konstantin; Tarasov, Andrey; Weller, Andreas

Published in:
Geophysical Journal International

DOI:
10.1093/gji/ggab071

2021

Document Version:
Publisher's PDF, also known as Version of record

Geophysical Journal International

Geophys. J. Int. (2021) **225,** 1982–2000
Advance Access publication 2021 February 19
GJI General Geophysical Methods

doi: 10.1093/gji/ggab071

Spectral induced polarization: frequency domain versus time domain laboratory data

Tina Martin [1], Konstantin Titov [2], Andrey Tarasov [2] and Andreas Weller [3]

[1] *Engineering Geology, Lund University, John Ericssons väg* 1, *SE*-22363 *Lund, Sweden. E-mail: tina.martin@tg.lth.se*
[2] *Department of Geophysics, Saint Petersburg State University, St Petersburg* 199034, *Russia*
[3] *Institute of Geophysics, Clausthal University of Technology,* 38678 *Clausthal-Zellerfeld, Germany*

Accepted 2021 February 17. Received 2020 December 22; in original form 2020 September 21

SUMMARY

Spectral information obtained from induced polarization (IP) measurements can be used in a variety of applications and is often gathered in frequency domain (FD) at the laboratory scale. In contrast, field IP measurements are mostly done in time domain (TD). Theoretically, the spectral content from both domains should be similar. In practice, they are often different, mainly due to instrumental restrictions as well as the limited time and frequency range of measurements. Therefore, a possibility of transition between both domains, in particular for the comparison of laboratory FD IP data and field TD IP results, would be very favourable. To compare both domains, we conducted laboratory IP experiments in both TD and FD. We started with three numerical models and measurements at a test circuit, followed by several investigations for different wood and sandstone samples. Our results demonstrate that the differential polarizability (DP), which is calculated from the TD decay curves, can be compared very well with the phase of the complex electrical resistivity. Thus, DP can be used for a first visual comparison of FD and TD data, which also enables a fast discrimination between different samples. Furthermore, to compare both domains qualitatively, we calculated the relaxation time distribution (RTD) for all data. The results are mostly in agreement between both domains, however, depending on the TD data quality. It is striking that the DP and RTD results are in better agreement for higher data quality in TD. Nevertheless, we demonstrate that IP laboratory measurements can be carried out in both TD and FD with almost equivalent results. The RTD enables a good comparability of FD IP laboratory data with TD IP field data.

Key words: Electrical properties; Numerical modelling; Time-series analysis.

INTRODUCTION

Almost 100 yr ago, the induced polarization (IP) effect was discovered by Conrad Schlumberger while doing geoelectrical DC measurements (Schlumberger 1920). He observed that after shutting off the injected current, the voltage was not dropping immediately down to zero but showing some decay, which he interpreted as capacitive behaviour of the underground. For years, this finding was used to localize and characterize ore mineral deposits by measuring strong polarization effects caused by electronic conductors and semi-conductors (e.g. Pelton *et al.* 1978; Wong 1979; Komarov 1980; Seigel *et al.* 2007).

With improvements of the measurement technique as well as of the processing and analysis tools, the field of application for the IP method had grown steadily. This enabled the IP method to become an important technique also for hydrogeological and environmental applications (e.g. Weller & Börner 1996; Binley *et al.* 2005; Kemna *et al.* 2012; Kessouri *et al.* 2019).

IP can be measured either in time domain (TD) or in frequency domain (FD), and in theory, these measurements should provide the same spectral information. Previous comparisons between TD IP and FD IP data have shown that they are similar but not equivalent because different parameters are measured in different frequency and time ranges (Zonge *et al.* 1972).

The gathering of spectral IP (SIP) information was done mainly in FD due to the higher accuracy and a wider bandwidth (e.g. Kemna *et al.* 2012). However, since more than a decade, spectral information can also be extracted from measurements in TD (Tarasov & Titov 2007; Fiandaca *et al.* 2013). In particular, it is quite common to measure high-accuracy FD IP data in a laboratory environment but using the TD IP technique in the field (e.g. Johansson *et al.* 2020). However, only very few studies have

addressed the different behaviour of TD and FD measurement data in the field (Flores Orozco *et al.* 2012; Maurya *et al.* 2018; Martin *et al.* 2020) and have compared laboratory FD IP and field TD IP measurements (Johansson *et al.* 2020). These results often reveal a strong difference between both measurement techniques in terms of data quality, acquisition time and instrument handling.

The aim of this paper is to compare TD and FD IP data sets obtained in a laboratory environment. We measured IP on samples of sandstone and wood in both TD and FD. By using numerical models and a test circuit, we were also able to prove our findings on a material-independent level. The use of the differential polarizability (DP) parameter enables a comparison of measured data from both domains. Furthermore, by using the Debye decomposition approach, we compared qualitatively the relaxation time distribution (RTD) for data sets obtained in both domains.

IP FUNDAMENTALS

While the conventional resistivity method focuses on the Ohmic conduction (or resistance), the IP method considers additionally polarization phenomena of natural material. The IP represents a reversible electrical charge accumulation subjected to an external electrical field and the charge relaxation towards the initial equilibrium state after the stimulating field is removed. The charge accumulation and depletion are processes that induce a secondary electrical field. The secondary field produces two phenomena, which manifest the IP and depend on the applied current: a decay of the voltage after removing of the external field (in TD) and a phase shift between the sinusoidal electrical current injected into a medium and the measured voltage (in FD).

The impedance, which is the complex voltage-to-current ratio, is measured and transformed into a complex electrical resistivity that results from a multiplication of the impedance by a geometrical factor, which depends on the geometry of the sample and the measuring cell,

$$\rho^* = K Z^* = K \frac{U^*}{I^*}, \tag{1}$$

where ρ^* is the resistivity in Ω m, Z^* is the impedance in Ω, K is the geometrical factor in m, U^* is the voltage in V and I^* is the current in A. All values marked by asterisks are complex values.

The complex resistivity can also be expressed by the absolute value, $|\rho^*|$, and the phase shift between voltage and current signal, ϕ,

$$\rho^* = |\rho^*| \exp(\mathrm{i}\phi), \tag{2}$$

or, alternatively, as the real, ρ', and imaginary, ρ'', parts of resistivity,

$$\rho^* = \rho' + \mathrm{i}\rho'', \tag{3}$$

with $\mathrm{i} = \sqrt{-1}$ being the imaginary unit, and

$$\tan(\phi) = \frac{\rho''}{\rho'}, \tag{4}$$

$$|\rho^*| = \sqrt{\rho'^2 + \rho''^2}. \tag{5}$$

By application of the electrical field at different frequencies (in theory from zero to infinity and with a continuous frequency distribution), one obtains the complete characterization of IP in FD.

In TD, the most common mode of measurements consists of injecting sequences of pulses of constant current and opposite polarity with pauses between them (usually of the same duration as the pulses) into the sample. The voltage is commonly measured between the pulses when the voltage decays. [Note that there are techniques with a sequence of pulses of different polarity without pauses and the voltage is recorded as a function of time (e.g. Madsen *et al.* (2017)].

The ratio of the voltage in pause $U_{\mathrm{off}}(t)$ (a so-called off-time, measured in V or in mV) to the voltage at the end of pulse U_{on} (on-time, in V) is defined as the polarizability at a certain time, $\eta(t)$, with

$$\eta(t) = U_{\mathrm{off}}(t) / U_{\mathrm{on}}. \tag{6}$$

The function $\eta(t)$ represents the dimensionless IP decay with the practical units of per cent or mV V^{-1}. In theory, by assuming a current step of infinite duration (from $t \to -\infty$ to $t \to 0$) one obtains a decay (with continuous measurements versus time), which completely characterizes IP in TD. The function $\eta(t)$ is always monotonically decreasing. It starts from the saturation value $\eta(0)$ (when $t \to 0$) and decreases to zero when $t \to \infty$.

In practice, measurements are conducted with different finite pulse lengths. Details about the reason of application of the pulses with different duration and the stack of responses of several pulses can be found, for example, in Titov *et al.* (2002) or Gurin *et al.* (2013, 2015).

Differential polarizability and transient characteristic

The derivative of the decay function $\eta(t)$ with respect to the time logarithm is defined as the DP (η_d; Komarov 1980; Titov *et al.* 2002),

$$\eta_d = -\frac{\mathrm{d}\eta(t)}{\mathrm{d}(\ln t)}. \tag{7}$$

Often, the DP contains a maximum or is (more or less) constant versus time, like the phase of the resistivity in FD. Therefore, the use of the DP results in a simpler way of analysing IP compared to the monotonous decays.

Considering the simple Debye relaxation process (Debye 1929), the polarizability after switching-off of the current step function can be written as

$$\eta(t) = m \cdot \exp(-t/\tau), \tag{8}$$

where m is the chargeability and τ is the relaxation time. The DP is then obtained:

$$\eta_d(t) = -\frac{\mathrm{d}\eta(t)}{\mathrm{d}\ln(t)} = -t \cdot \frac{\mathrm{d}\eta(t)}{\mathrm{d}t} = m \cdot \frac{t}{\tau} \exp(-t/\tau). \tag{9}$$

This function contains a maximum whose position along the time axes coincides with the value of τ. The maximum magnitude is

$$\max(\eta_d) = m/e, \tag{10}$$

with e being the Euler's number (mathematical constant, approx. equal to 2.71828).

In practice, the simple discrete form can be used to calculate the DP:

$$\eta_d(t_j) = -\frac{1}{2}\left(\frac{\eta_j - \eta_{j-1}}{\ln(t_j/t_{j-1})} + \frac{\eta_{j+1} - \eta_j}{\ln(t_{j+1}/t_j)}\right), \tag{11}$$

where the index j corresponds to the discrete values of time.

When the current pulses of opposite polarity are used to stimulate IP in TD, the full current waveform (pulse and pause durations) influences the magnitude and shape of IP decays. For a Debye

relaxation (eq. 8), an analytical expression can then be obtained by

$$\eta(t) = m \cdot \exp(-t/\tau)\,[(1-\exp(-T/\tau)) \times \frac{1-\exp(-2T/\tau)+\exp(-4T/\tau)}{1-\exp(-4T/\tau)}], \quad (12)$$

where T is the duration of the off-time and the on-time. The derivation of eq. (12) can be found in Appendix C.

In FD, in terms of the resistivity, the Debye model is written as

$$\rho^*(\omega) = \rho_0\left(1 - m\left(1 - \frac{1}{1+\mathrm{i}\omega\tau}\right)\right), \quad (13)$$

where ρ_0 is the low-frequency limit of the resistivity (in Ωm), $\omega = 2\pi f$ is the angular frequency (in rad s^{-1}) and f is the frequency (in Hz). The real part of the complex resistivity is given as

$$\rho' = \rho_0\left(1 - m\frac{(\omega\tau)^2}{1+(\omega\tau)^2}\right), \quad (14)$$

and the imaginary part is

$$\rho'' = \rho_0 m\frac{\omega\tau}{1+(\omega\tau)^2}. \quad (15)$$

The resistivity phase is then written as

$$\phi(\omega) = \mathrm{atan}\left(-\frac{m\omega\tau}{1+(1-m)(\omega\tau)^2}\right). \quad (16)$$

For small values of the phase (less than 100 mrad), eq. (16) becomes

$$\phi(\omega) \approx -\frac{m\omega\tau}{1+(1-m)(\omega\tau)^2}. \quad (16a)$$

From eq. (16a), we get the frequency of the phase maximum (max($-\phi$)) (Tarasov & Titov 2013) with

$$\omega = \frac{1}{\tau}\frac{1}{\sqrt{1-m}}, \quad (17)$$

and

$$\max(-\phi) = \frac{m}{2\sqrt{1-m}}. \quad (18)$$

By comparing both eqs (10) and (18), a nearly linear relationship between the phase and the DP can be observed for varying values of m (see Fig. 1). Considering the Debye model, we find that DP = 1 per cent corresponds to $\phi = -13.7$ mrad (for $m = 0.027$). However, this transformation is only valid for a Debye model with low m.

For a Pelton model (Pelton *et al.* 1978), the DP/ϕ ratio is changing slightly due to the dimensionless exponent c. This model can be presented as (e.g. Kemna 2000)

$$\rho^* = \rho^\infty + \frac{\rho^0 - \rho^\infty}{1+(\mathrm{i}\omega\tau)^c}, \quad (19)$$

with ρ^∞ being the high-frequency limit of the resistivity (in Ωm), and the exponent c ($0 < c \leq 1$) characterizes the shape of the phase curve and depends on the width of the RTD. A larger c corresponds to a more accentuated phase peak. For $c = 1$, eq. (19) becomes equal to eq. (13). Therefore, the Pelton model (four parameters) is the extension of the Debye model (three parameters). The parameter τ is referred to as time constant (Pelton *et al.* 1978). The chargeability m is defined by the high- and low-frequency limits of the resistivity in the following way:

$$m = \frac{\rho^0 - \rho^\infty}{\rho^0}. \quad (20)$$

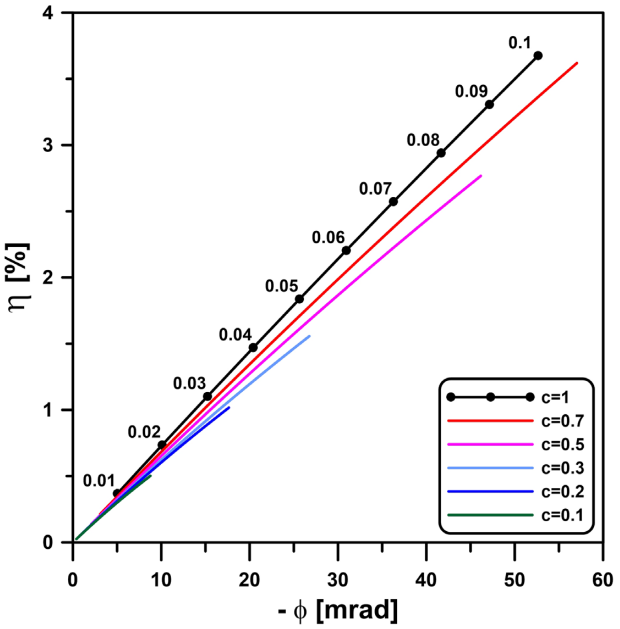

Figure 1. DP versus phase for a Debye model and various Pelton models for small m (black numbers) and varying c (coloured lines).

Using the analytic expression for the polarizability decay (Komarov 1980) for a Pelton model with $c = 0.5$, we obtain

$$\eta(t) = m \cdot \exp(t/\tau)\mathrm{erfc}\left(\sqrt{t/\tau}\right), \quad (21)$$

where erfc(x) is the probability integral. We obtain the maximal DP magnitude and the position of the maximum along the time axis by

$$\eta_d(t) = -m \cdot \frac{t}{\tau}\left(\exp(t/\tau)\mathrm{erfc}\left(\sqrt{t/\tau}\right) - \frac{1}{\sqrt{\pi\frac{t}{\tau}}}\right). \quad (22)$$

Considering eqs (21) and (22), we get for DP = 1 per cent a phase angle $\phi = -15.8$ mrad for $c = 0.5$. Therefore, the DP/ϕ ratio depends on c and is valid for small m. Furthermore, the position of the maximum of the DP magnitude is also affected by c. In the case of a Pelton model with c = 0.5, we get the maximum at $t = 0.67\ \tau$. A detailed discussion about the influence of c can be found in Appendix A.

For an arbitrary Debye model, the polarization response can be calculated for both FD and TD, as shown in Fig. 2 in terms of the polarizability decay and DP (Fig. 2a), and in terms of resistivity amplitude and the phase (Fig. 2b). We observe very similar shapes for the curves of DP and phase. Scaling the axis in accordance with the comparison in Fig. 1 (DP = 1 per cent corresponds to $\phi = -13.7$ mrad), we get a comparable magnitude of the DP and phase curves. Nevertheless, while the phase curve is exactly symmetrical for the Debye model, the DP curve is slightly asymmetric. That means that a certain similarity between DP and phase curve can be achieved but not equivalent curves.

Relaxation models

To date, there is no consensus regarding a universal model describing IP (even phenomenologically). A common way is the application of the complex resistivity Pelton model (see above, eqs 19 and 20).

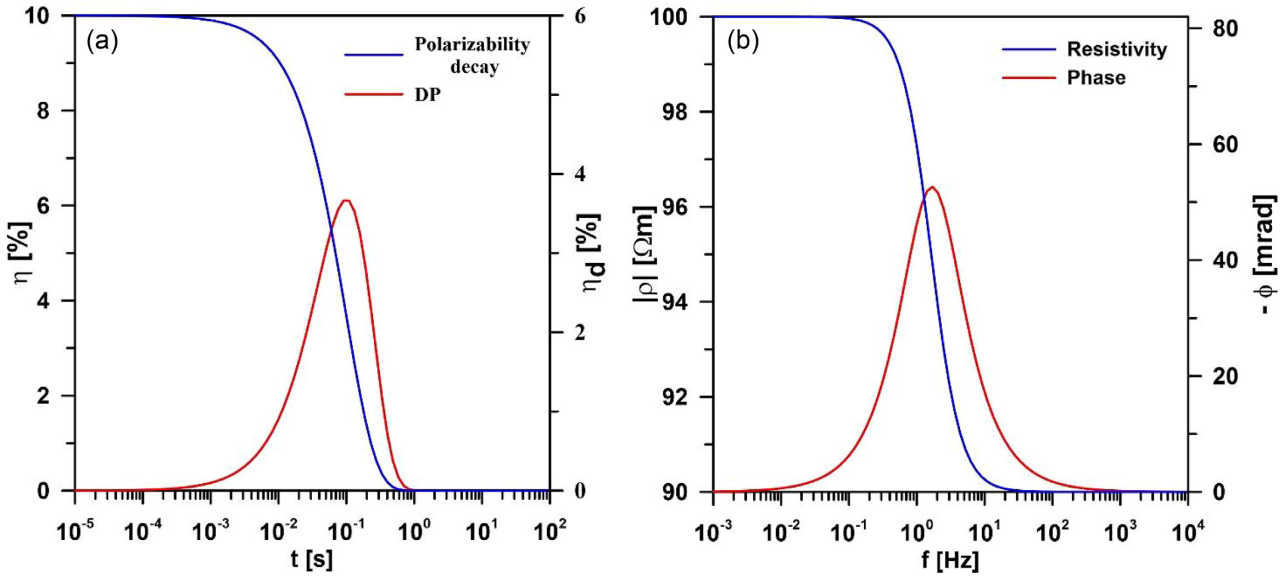

Figure 2. Debye polarization in TD and FD. (a) Polarizability decay and DP; (b) resistivity and phase. The parameters are $m = 0.1$, $\tau = 0.1$ s and $\rho_0 = 100$ Ωm. The vertical axes were scaled considering the relationship that 1 per cent DP corresponds to −13.7 mrad to get a similar magnitude of the curves.

Alternatively, IP data can be fitted to the Cole–Cole model (Cole & Cole 1941), which was initially proposed for the complex dielectric constant and is also formulated for the complex electrical conductivity as

$$\sigma^* = \sigma^0 + \frac{\sigma^\infty - \sigma^0}{(1 + \mathrm{i}\omega\tau)^c}, \tag{23}$$

where σ^0 and σ^∞ are the low- and high-frequency limits of the electrical conductivity (in S m^{-1}), respectively. In analogy to eq. (20), the chargeability m is determined by

$$m = \frac{\sigma^\infty - \sigma^0}{\sigma^0}. \tag{24}$$

The resulting parameters of the Cole–Cole model are close to those of the Pelton model for sufficiently low chargeability values (Tarasov & Titov 2013). However, experimental phase spectra can contain multiple peaks or can be almost constant. In such cases, multiple Pelton or Cole–Cole models (e.g. Kemna 2000; Kemna *et al.* 2012), or a constant phase angle model (Börner & Schön 1991), can be applied to fit the data.

A universal and elegant way of approximation of experimental data is their transformation to an RTD. This RTD can be defined based on the superposition of the Debye models in both FD (e.g. Nordsiek & Weller 2008),

$$\sigma^*(\omega) = \sigma^0 \left(1 + \int_0^\infty \frac{m_p(\tau)\,\mathrm{d}\tau}{1 + \mathrm{i}\omega\tau}\right), \tag{25}$$

and TD (e.g. Tarasov & Titov 2007)

$$\eta(t) = \int_0^\infty m_p(\tau) \exp\left(-\frac{t}{\tau}\right) \mathrm{d}\tau. \tag{26}$$

Here, the dimensionless function $m_p(\tau)$ is defined as the partial chargeability (see Nordsiek & Weller 2008) or the RTD (see Tarasov & Titov 2007). Eqs (25) and (26) must be solved for $m_p(\tau)$. These equations represent Fredholm equations of second kind. The determination of $m_p(\tau)$ represents an ill-posed problem that can be solved based on the Tikhonov regularization approach (Tikhonov & Arsenin 1977) that assumes typically a smoothness constraint RTD. The integral

$$m = \int_0^\infty m_p(\tau)\,\mathrm{d}\tau, \tag{27}$$

yields the total chargeability, which is a measure of the IP magnitude. In this study, we transform resistivity spectra and IP decays to RTDs.

MATERIALS AND METHODS

Instruments and sample holder

We carried out the TD measurements with the AIE-2 instrument [*Astra Geo*, St. Petersburg, Russia—see also Gurin *et al.* (2013) for the instrument description and tests]. We used a laboratory transmitter that injects the current between 1 and 1000 μA into samples with a maximum output voltage of 10 V. To measure the voltage, we used a custom-made pre-amplifier to increase the input resistance of the instrument. The pulse and pause durations are selected between 1 and 64 s with a signal form of positive pulse–pause–negative pulse–pause.

We used the instrument SIP Fuchs III (Radic Research 2019, Berlin, Germany) for the FD measurements. This instrument enables measurements of the impedance in a frequency range from 1 mHz to 20 kHz. It includes an internal 50 W transmitter and uses two remote reference units (RRU). We injected sinusoidal current signals with a maximum of 0.7 mA.

We also obtained data with the PSIP instrument (Ontash & Ermac 2018, New Jersey, USA). Here, the SIP response is measured by applying sine wave in the frequency between 1 mHz and 20 kHz. For both FD instruments, the amplitude and phase of the impedance are determined from the time-series of injected current and measured voltage.

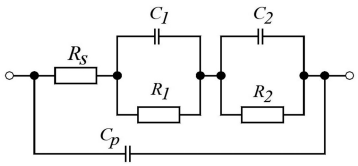

Figure 3. Test circuit (modified from Zimmermann 2010).

Table 1. Debye parameters for the test circuit (Zimmermann 2010).

R_0 (Ω)	m_1 (-)	m_2 (-)	τ_1 (μs)	τ_2 (s)	Peak f_1 (Hz)	Peak f_2 (Hz)
165 360	0.031	0.060	11.19	0.22	14 223	0.72

Table 2. Parameters of the numerical models based on the Pelton model.

Model	# of terms	ρ_0 (Ωm)	m (-)	τ (s)	c (-)
1	1	100	0.1	0.1	0.5
2	2	50	0.1	0.5	0.8
		50	0.05	0.05	0.8
3	2	100	0.1	0.05	0.3
		100	0.05	5	0.3

We used a four-point measuring cell as sample holder as described in Kruschwitz (2007). It includes stainless steel plate electrodes for the current injection and silver-wire ring electrodes for the potential measurements. The shape of the sample holder was either cylindrical or square-shaped, depending on the shape of the samples. Agar gel was used as a coupling agent.

Material

Test circuit

We used the test circuit ZEL-SIP-T03, which originally was provided by the Research Centre Jülich for the German IP working group to conduct a round robin test. Originally, this test circuit was presented by Vanhala & Soininen (1995) to imitate natural soil samples. It consists of a serial and parallel connection of resistors and capacitors (Fig. 3). The respective Debye model parameters for the two sum terms are shown in Table 1 (Zimmermann 2010).

In FD, we measured the impedance in a frequency range between 1 mHz and 20 kHz with both instruments (SIP Fuchs III and PSIP). Due to some disturbances in the laboratory setup during the SIP Fuchs III measurementsat the test circuit, the high frequency range from 100 Hz to 20 kHz was disturbed for the SIP Fuchs III instrument. Hence, we used the PSIP data set for the comparison between TD and FD for the test circuit. For all following data sets we used the FD data from the PSIP instrument .

In TD, we probed the test circuit with different pulse lengths (1, 2, 4, 8, 16, 64 s) and stacking numbers [10 (for 1, 2, 3 s), 8 (for 8 s), 6 (for 16 s) and 4 (for 64 s)] using a current of 5 μA.

Numerical models

We used three numerical Pelton models with varying parameters.

Model 1 has a single Pelton term. Models 2 and 3 represent a sum of two Pelton terms (see Table 2). We suppose that these models imitate more realistic IP responses in comparison to the test circuit.

We used the fast Hankel transform to calculate the IP decay (Fiandaca *et al.* 2013). The polarizability decays after a series of current pulses with opposite sign, and with the duration, T, reads (Tarasov & Titov 2007)

$$\widehat{\eta}\,(t,\,T,\,N) = \sum_{n=0}^{N-1} (-1)^n \left[\eta\,(t + 2nT) - \eta\,(t + (2n+1)\,T)\right], \quad (28)$$

where η is the polarizability after the infinity-length current pulse as the result of the fast Hankel transform of eq. (12), t is the time after the moment of switching-off of the last pulse, N is the number of pulses (which must have been an even number due to the fact that the AIE instrument always uses pair pulses to account for the spontaneous polarization of the potential electrodes).

The used parameters for the calculated IP decays are listed in Table 3.

Wood samples

To cover varying phase behaviour, we have chosen four tree species (oak (Q), lime (Ti), poplar (Po) and beech (Fa), see Fig. 4a). These samples, which have been investigated in previous studies (Martin 2012, Martin *et al.* 2015), were taken several years ago and stored during this time in dry condition. The shape of the samples is blocky being 20 mm in both height and width, but the samples differ in length. More information about the wood samples can be found in Martin *et al.* (2015). For each tree species, we measured two samples several times in the frequency range between 0.001 and 1000 Hz, but we show only the results of one sample due to the result similarity and for the sake of brevity. Before the measurements, all samples were saturated under vacuum with NaCl solution with a conductivity of 0.1 Sm^{-1}. After saturation, the samples were stored for two weeks to reach equilibrium between the tissue and the brine.

We carried out the TD measurements with the same pulse lengths and stacks as for the test circuit but using a current of 100 μA (see also Table A1 in the Appendix A).

Sandstone samples

We measured five sandstone samples: Röttbacher (Roett), Baumberger (Baum), Santa Fiora (SF), Oberkirchner (OK) and Langenauer (Lan, see Fig. 4b). We have chosen these geological samples due to their different polarization properties, which have been described in detail by Zhang *et al.* (2018) and Kruschwitz *et al.* (2020). The size of all samples was either 20 mm in diameter and 70 mm length for the cylindrical sample or 20 mm width × 20 mm height × 70 mm length for the Langenauer sample. The sandstone samples were saturated under vacuum with an NaCl brine with a conductivity of 0.1 $S\,m^{-1}$. After saturation, the samples were stored in the fluid for two weeks to reach an equilibrium between the solid and

Table 3. Parameters for the calculation of the polarizability decays for the three numerical models.

Pulse length (s)	1	2	4	8	64
Stacks (-)	32	16	16	8	4
Time range t_{min}–t_{max}, (s)	10^{-5}–0.9	10^{-5}–1.8	10^{-5}–3.6	10^{-5}–7.2	10^{-5}–57.6

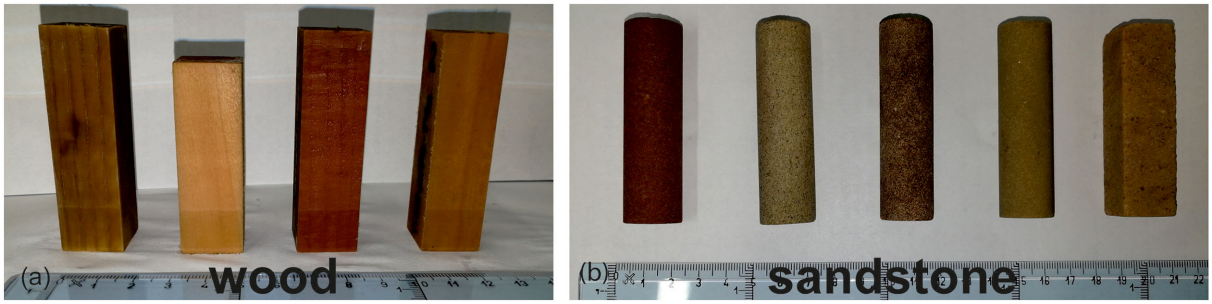

Figure 4. Photographs of (a) the measured wood samples and (b) sandstone samples.

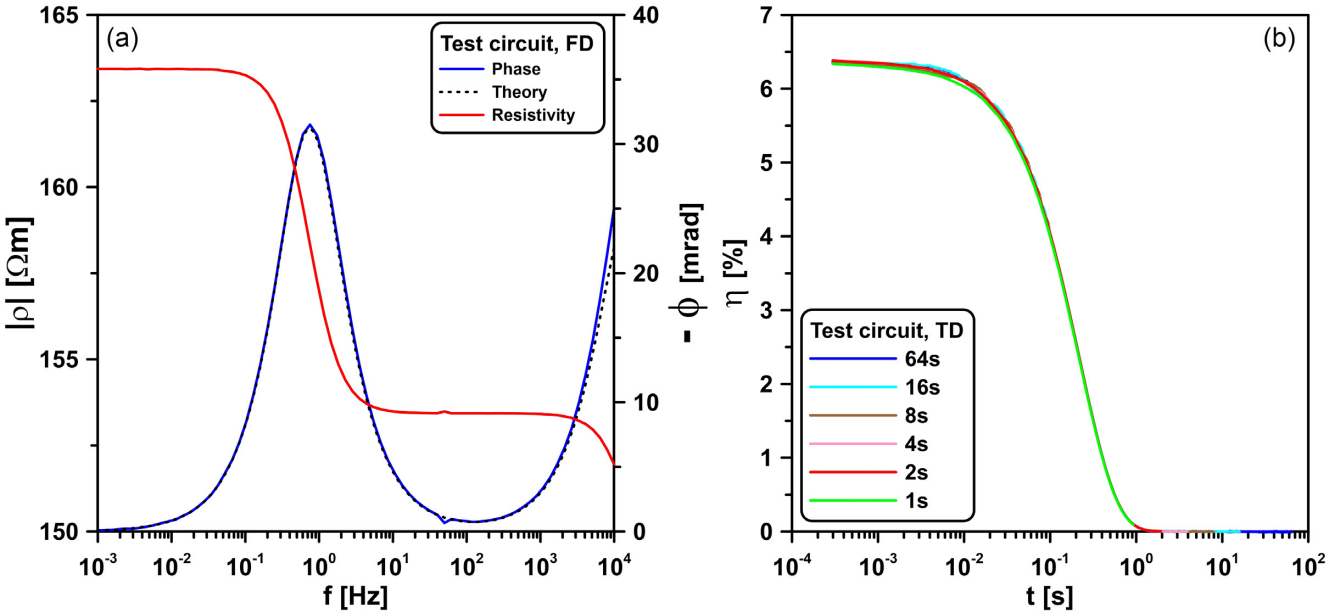

Figure 5. (a) Measured IP spectra [amplitude of resistivity (red) and phase (blue)] and (b) IP decay curves for different pulse lengths for the test circuit.

liquid phases before the IP measurements were carried out. While all samples were measured in the entire frequency range (0.001–1000 Hz), the Langenauer sample was measured in the frequency range between 0.01 and 1000 Hz due to time problems in the laboratory. The TD measurements were also carried out with the same pulse lengths and stacks as for the test circuit using the current value of 10 μA due to the higher resistivity than that of the wood samples (see Table A2 in Appendix A).

RESULTS

First, we present the measured raw data as decay curves (in TD) as well as the amplitude and phase of the complex resistivity (in FD). Thereafter, we show the DP curves, which are calculated from the polarization decay for different pulse lengths (eq. 12). Transferring the DP timescale into the frequency scale ($f = (2\pi t)^{-1}$), these values will be directly compared with the phase shift. Finally, by using smoothed decay curves, the TD data are transformed to RTD using the Debye model as the kernel function in the integral equation (eq. 26). The RTDs obtained from both domains will be shown together for different samples.

Raw data

Test circuit and numerical models

The measured curves for the test circuit are shown in Fig. 5 for (a) amplitude and phase spectra of the complex resistivity in FD and (b) the polarizability decay in TD. The FD data are in a perfect match with the theory: the first phase peak was reached at the

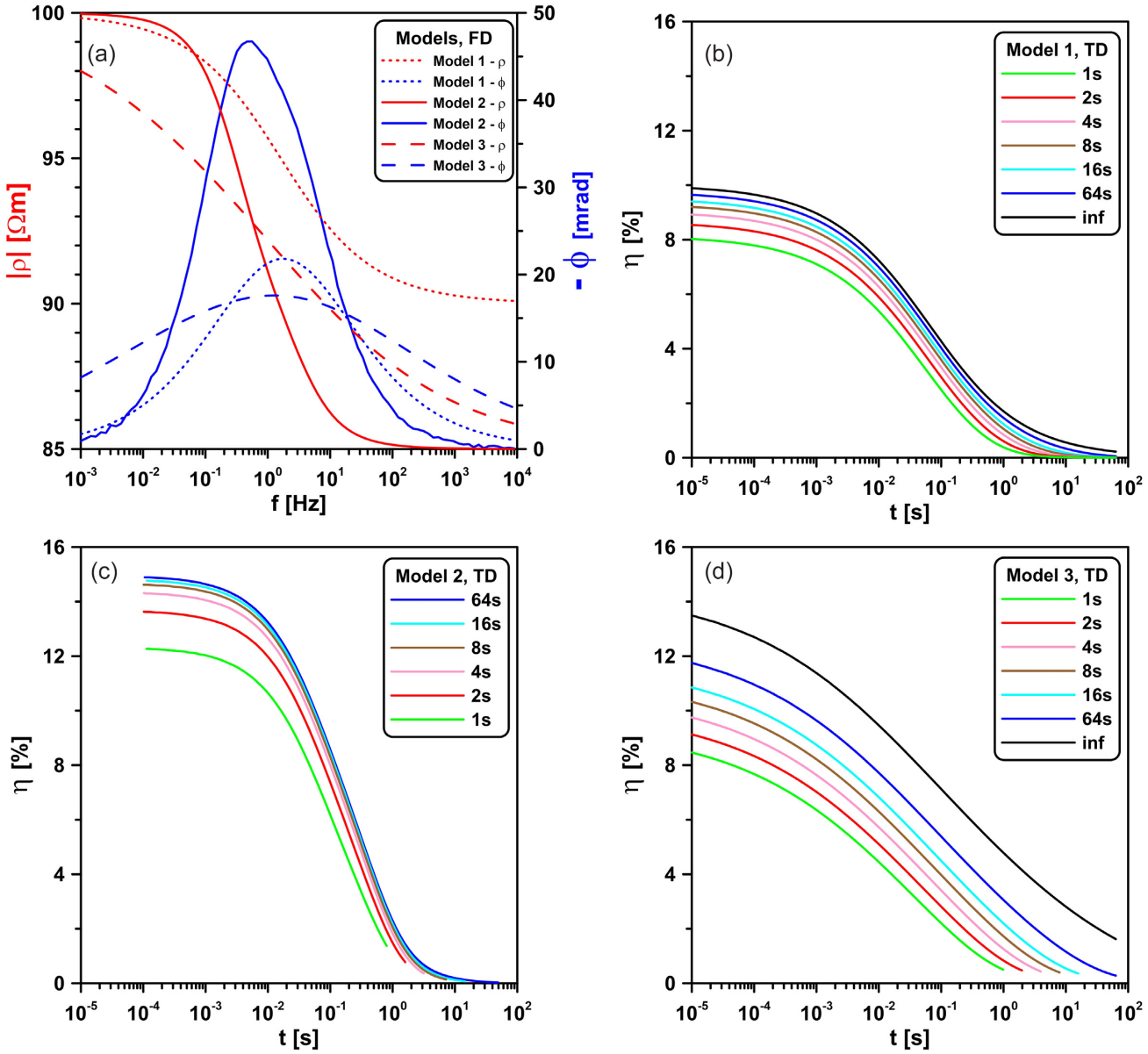

Figure 6. (a) Simulated IP spectra for all three numerical models and TD IP data for (b) Model 1, (c) Model 2 and (d) Model 3.

frequency $f = 0.75$ Hz while the second peak is out of the measured frequency range. In TD, the decay curves for all pulse lengths are similar and the signals reach the noise level latest after 2 s.

In Fig. 6, we show the simulated FD and TD data for the three numerical models. Model 1 shows a symmetric phase curve with a maximum at 1.6 Hz (Fig. 6a—fine dashed lines). The TD decay curves depend on the pulse length and reach their maximum polarizability for an infinity pulse length (inf—Fig. 6b). For Model 2, the first phase peak (Fig. 6a—continuous line) is very well pronounced (at $f = 0.3$ Hz), while the second one can be surmised by the asymmetric hunch of the phase spectrum at higher frequencies (at approximately $f = 3$ Hz). In TD (Fig. 6c), the same shape of the decay curve can be observed, but the magnitude of the polarizability value increases with the pulse length. Model 3 shows a much broader phase curve (Fig. 6a—rough dashed line) due to the low value of c. Similar to Model 2, both Pelton terms cannot be discriminated, and only a slight asymmetry can be observed. Compared to the TD results from both previous models, the decay curves (Fig. 6d) looks flatter.

Wood

The FD IP results for the four investigated wood samples are displayed in Fig. 7. All samples show resistivity amplitudes between 10 and 60 Ωm and a slight decrease of the resistivity with an increase in frequency. All phase spectra contain well-pronounced maxima with the peak frequency in the range from 0.01 to 1 Hz. The magnitude of the phase reaches peak values between −20 and −40 mrad.

Due to the large number of measurements in TD, only a selection of decay curves is shown in Fig. 8. The decay curves for all measured pulse lengths for the beech sample are presented in Fig. 8(a). These data show very smooth behaviour. In accordance with the

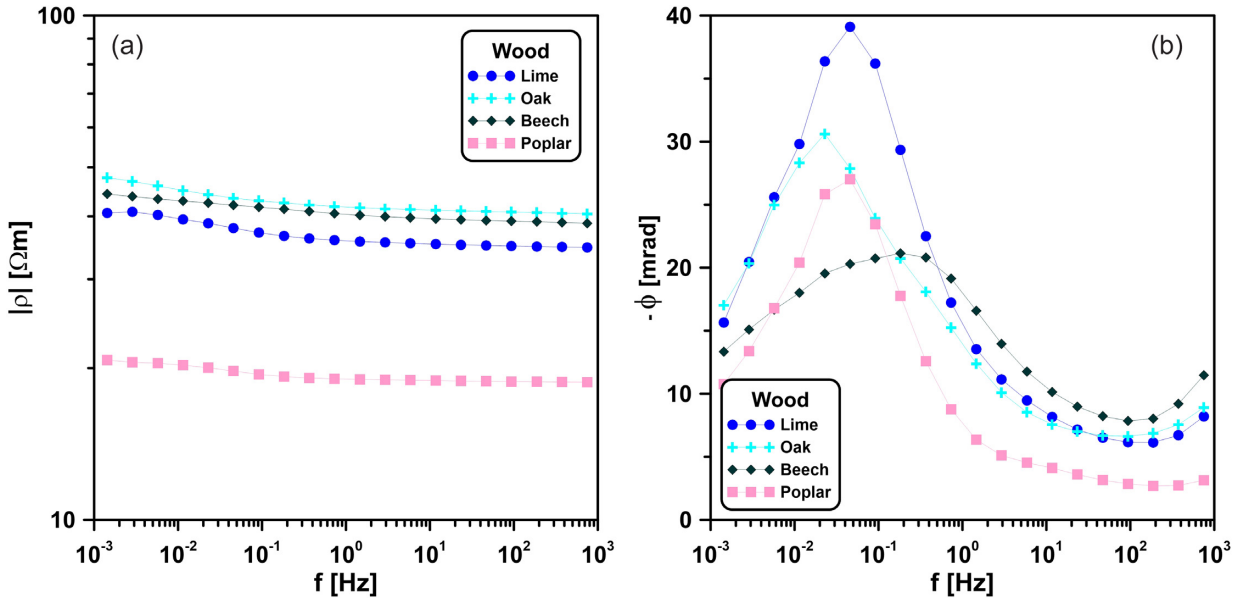

Figure 7. IP spectra for the four different wood species samples: (a) amplitude of resistivity; (b) phase.

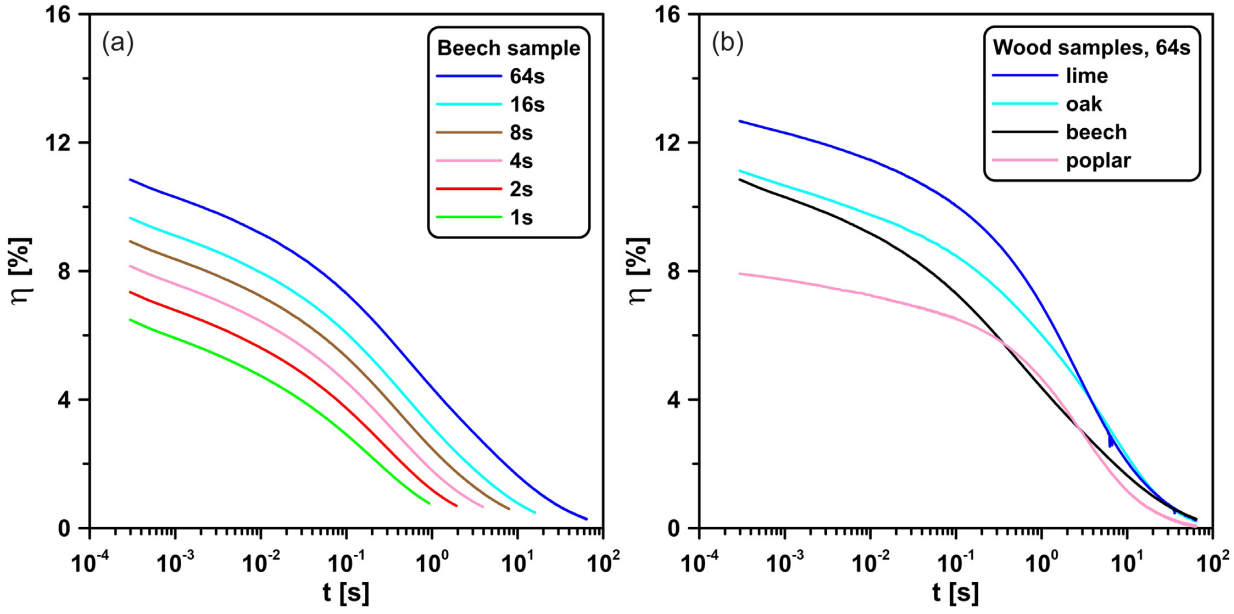

Figure 8. TD IP data for (a) the beech sample measured with pulse lengths from 1 to 64 s and (b) for all wood samples with a pulse length of 64 s.

numerical models, the polarization magnitude at early times indicates an increase with longer pulse lengths. Fig. 8(b) shows the 64 s pulse length decay curves for all four wood samples. Here, the signal quality in terms of repeatability and smoothness is very good for all samples. Only rarely, minor noise was found (i.e., lime sample—blue line at late times). The shape of the decays differs between the tree wood species.

The resistivity results from the TD measurements for all pulse lengths are listed in Table A1 in Appendix A. Obviously, the resistivity increases with increasing pulse length. By comparison of the TD resistivity for the longest pulse (64 s) with the low-frequency resistivity, obtained in FD, the values are similar and reaches a maximum deviation of 14 per cent, which can be explained by the too small pulse lengths (64 s) in contrast to the measured low frequency (0.01 Hz) in FD.

Sandstone

The IP spectra of the investigated sandstone samples are presented in Fig. 9. The wide variation in the phase spectra (Fig. 9b) indicates the variability of the polarization behaviour of the sandstone samples. The Langenauer (Lan) sample show a clear double peak at frequencies $f = 93$ Hz and $f = 0.02$ Hz with higher phase values (> 30 mrad), while the Röttbacher (Roett) and Oberkirchner (OK) samples show single phase peaks. The Santa Fiora (SF) and Baumberger (Baum) samples show a more or less continuous increase of the phase with increasing frequency.

The TD decay curves for the Langenauer (a), Oberkirchner (b) and all sandstone samples at the pulse length of 8 s (c) are shown in Fig. 10 since the data quality for the pulse length of 64 s were not sufficient for some of the sandstone samples. Only the data quality

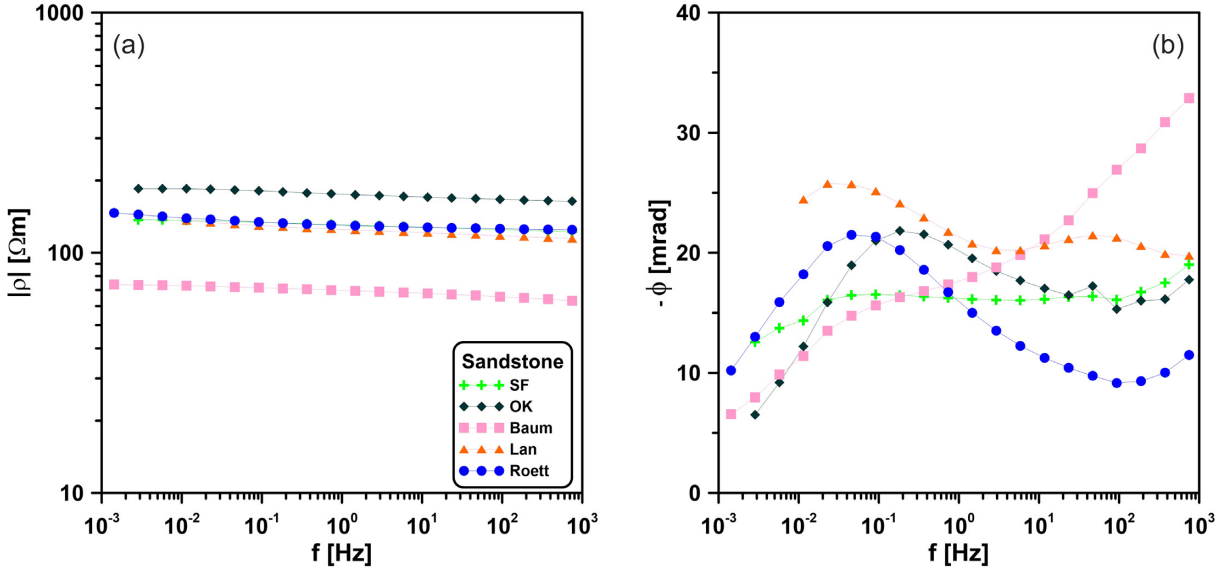

Figure 9. IP spectra for the sandstone samples: (a) amplitude of the resistivity; (b) phase.

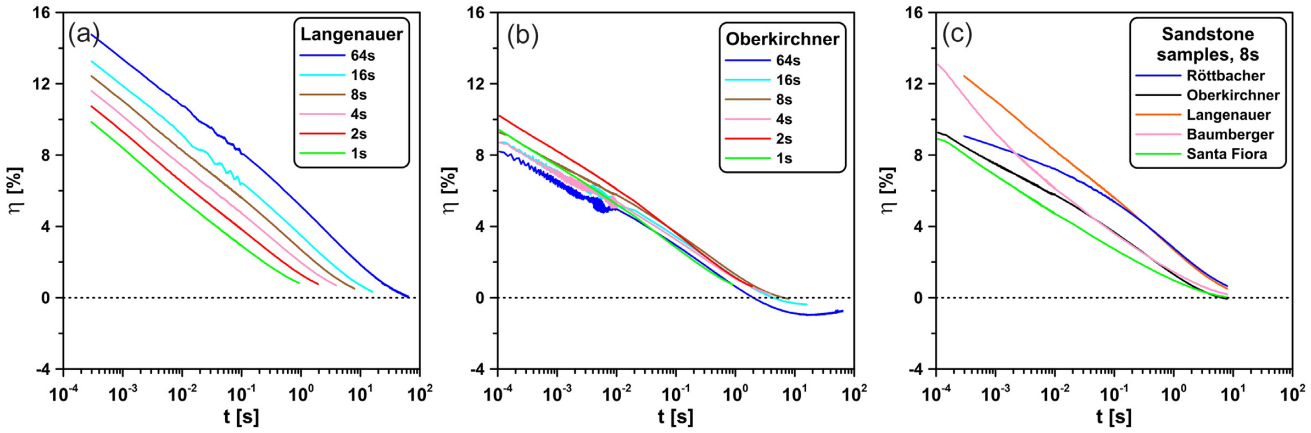

Figure 10. TD IP data for (a) the Langenauer and (b) the Oberkirchner samples measured with the pulse length from 1 to 64 s, and (c) for all sandstone samples with 8 s pulse length. The oscillation at long pulse lengths (>16 s) might be caused by electrode instabilities (e.g. due to polarization processes).

for the Langenauer (see Fig. 10a) and Röttbacher samples was very good and comparable with the data quality obtained with the wood samples. In contrast, the data for the Oberkirchner (Fig. 10b), Santa Fiora and Baumberger samples show some noise and also negative values were gathered for long pulse lengths (>8 s). In accordance with the FD results, the sandstone samples differ also in the shape of their decay curves (see Fig. 10c, for the 8 s pulse length).

To complete the results, the settings and resistivity values for the sandstone samples can be found in Table A2 in Appendix A. The TD resistivity values are largely in agreement with the resistivity from the FD measurements with a maximal deviation of 9 per cent.

Differential Polarizability

To compare the raw data between TD and FD, we have calculated the DP η_d from the decay curves (see above) and plotted the DP versus frequency calculated as $f = (2\pi t)^{-1}$. Now, a direct visual comparison between the phase and DP is possible and will be shown for the test circuit, the numerical models, as well as for the wood and sandstone samples.

Test circuit and numerical models

In Fig. 11, the DPs for different pulse lengths (coloured lines) are shown in one graph with the phase data from the FD measurements (black dashed line) for both the test circuit (a) and the three numerical models (b, c, d). We scaled the vertical η_d- and ϕ-axes in Fig. 11(a) considering a DP/ ϕ ratio with 1 per cent in DP corresponding to 13.7 mrad in $-\phi$ as identified by a comparison of eqs (10) and (18) for a Debye model (see Fig. 1). In this case, the curves for DP and phase as well as the position of both peaks match almost perfectly. The low-frequency maximum can be observed at $f = 0.74$ Hz in the phase curve and at $\tau = 0.22$ s in the DP curve. According to the theory (see Fig. 2), an asymmetric shape of the DP at lower frequencies can be recognized.

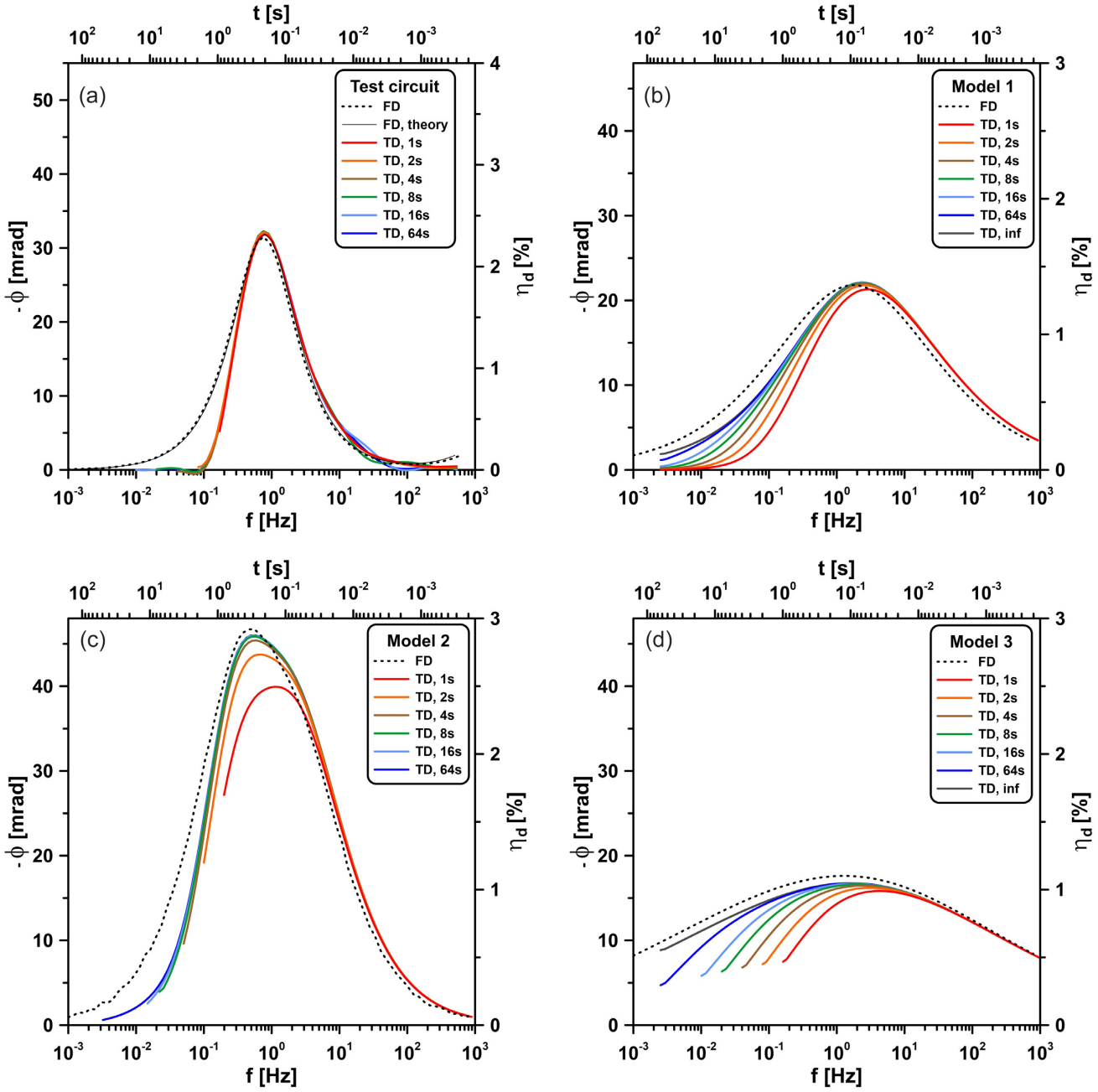

Figure 11. Phase shift (left axis) and DP (right axis) for (a) the test circuit and (b–d) the three numerical models. According to the IP fundamentals, the vertical axis in (a) was scaled with the DP/ ϕ ratio 1 per cent/−13.7 mrad, while the axes in (b)–(d) were scaled with a DP/ϕ ratio 1 per cent/−16 mrad.

For the comparison of DP and phase curves for the Pelton models and all following natural samples, a DP/ ϕ ratio 1 per cent/−16 mrad was used for the scaling of the vertical axis. This value enables a better agreement for models with lower c – values as shown in Fig. 1. In general, the shapes of DP and the phase curves are very similar for all numerical models (Figs 11b–d), in particular for the high frequency range (>10 Hz). Due to the used DP/ ϕ ratio for $c = 0.5$, in particular for Model 1 (Fig. 11b), the maxima of the two curves are in very good agreement. Small discrepancies can be seen for Model 2 and Model 3. Due to the effect of the finite pulse lengths and of the linear combination of strong asymmetrical DP responses, the calculated DP are also shifted slightly along the vertical axes.

Wood

A comparison of DP and phase curve for the wood samples is shown in Fig. 12. Independently of the pulse length, the DP curves are in very good agreement with the phase curve (see Fig. 12a for the lime sample). The magnitudes of DP and phase are very similar. Only a slight shift for the position of the peak exists. However, measurements with short pulse lengths cannot resolve the polarization maximum at low frequencies. So, the longer the pulse, the more information in the low-frequency range can be extracted (from 10^{-3} Hz to 10^{-2} Hz). Therefore, the DP curves for all the four wood samples for the 64 s pulse are displayed in Fig. 12(b). They are all in good agreement with the respective phase curves.

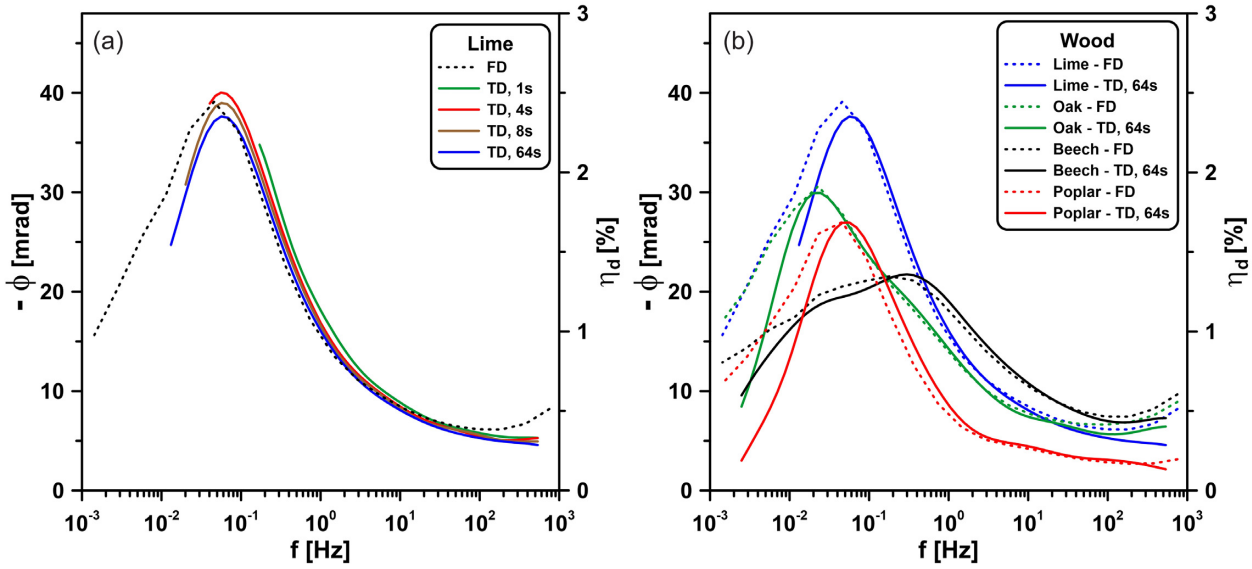

Figure 12. DP and phase shift for several pulse lengths for (a) the lime sample and (b) all wood samples at pulse length 64 s. The vertical axes were scaled with a DP/ϕ ratio 1 per cent/−16 mrad.

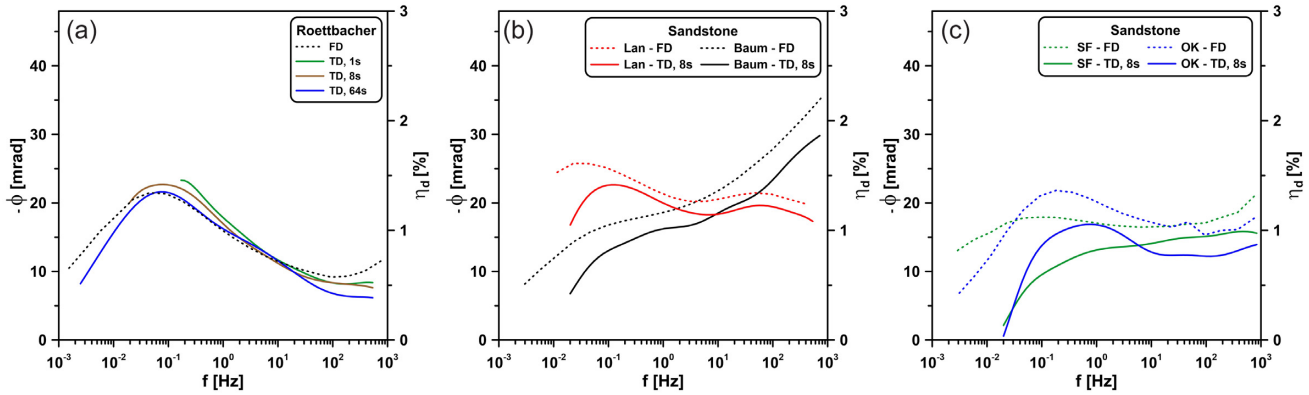

Figure 13. DP and phase shift for several pulse lengths for (a) the Röttbacher sample, (b) the Langenauer and Baumberger samples and (c) the Santa Fiora and Oberkrischner samples at the pulse length of 8 s. The vertical axes were scaled with a DP/ϕ ratio 1 per cent/−16 mrad.

Sandstone

For the sandstone samples, the DP and phase curves are shown in Fig. 13. For the samples with sufficient data quality, the curves show good similarity (Fig. 13a for the Röttbacher sample). For the samples with minor data quality at long pulse lengths (>8 s, e.g. OK, SF, Lan), larger differences can be observed (Figs 13b and c). Even though the shapes of the curves are similar and show one or two peaks at similar frequencies, a slight shift of the maxima to higher frequencies for TD can be recognized.

Relaxation time distribution

To compare the data qualitatively, we calculated the RTD from both FD and TD data using the Debye decomposition approach using a code as described in Weigand & Kemna (2016) in FD, and Tarasov and Titov (2007) in TD.

We fitted FD and TD data within the same time/frequency bandwidth, and with identical time windows. For the inversion of the TD data for the natural samples (wood and sandstone), we used the data from three different pulse lengths: 1 s for the short pulses, 4 s or 8 s for the medium pulse length and 64 s for the long pulses. The results shown here follow the same order as before.

Test circuit and numerical models

In Fig. 14, the RTDs for the test circuit (a) and the numerical models (b–d) are presented. Gaussian noise had been added to numerical model data. For the TD data we added noise to the polarizability decays with a standard deviation (sd) of 10^{-2} per cent. For the FD phase data, we added the noise with sd = 0.16 mrad.

We used a joint inversion of resistivity amplitude and phase for the FD data. In both cases (FD and TD), the same time range from 10^{-6} to 3×10^{3} s was used with 40 relaxation time values (for more information see Tarasov & Titov 2007).

As shown in Fig. 14, the RTDs from FD and TD are in very good agreement for both the magnitude and the peak position. Only for the test circuit RTDs (Fig. 14a), a very small discrepancy for the TD RTD at the lower time range is detected which is within the limits of uncertainty.

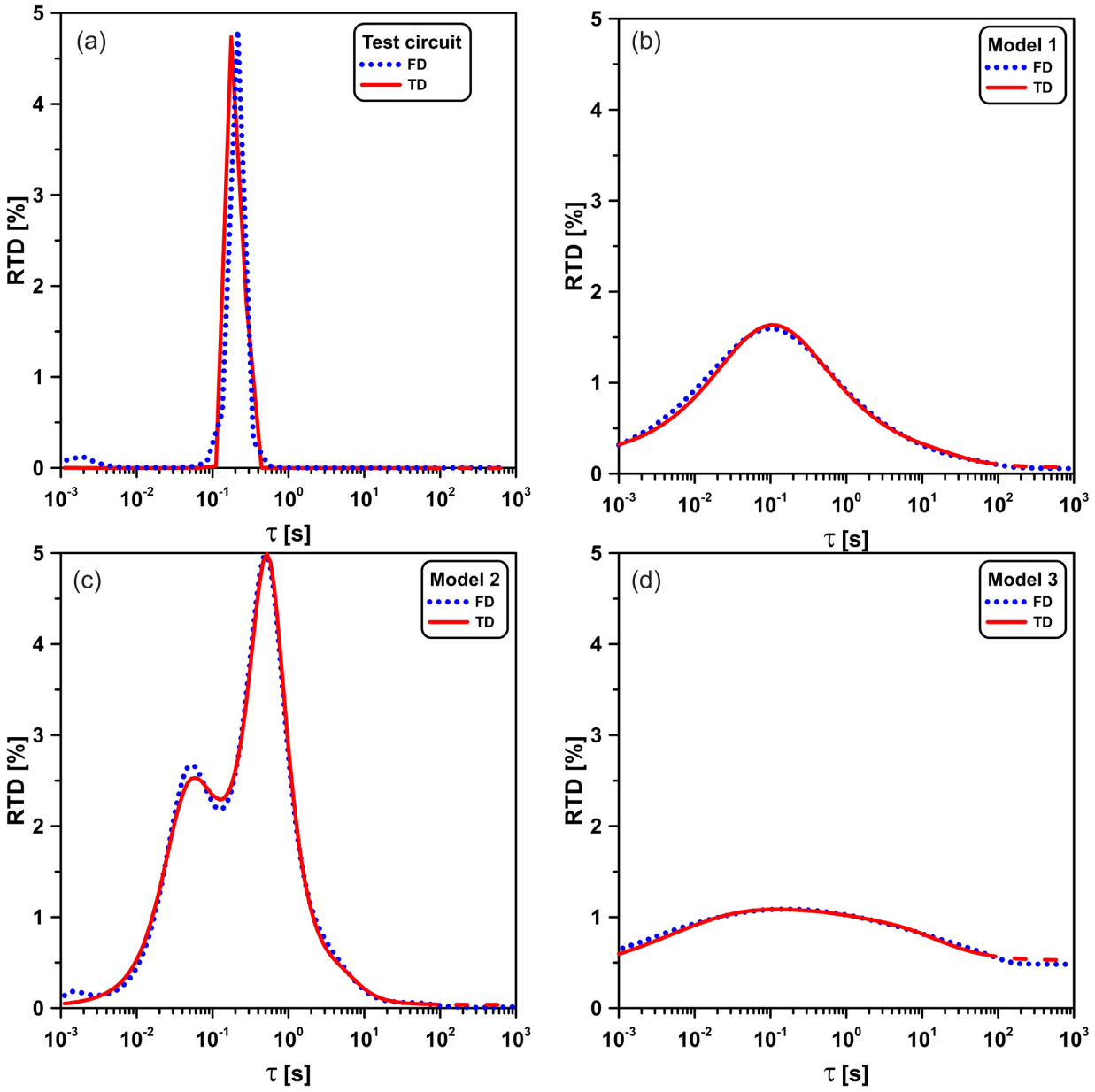

Figure 14. RTD for (a) the test circuit and (b–d) the three numerical models. The dashed lines for higher relaxation times in TD represent extrapolated curves because the longest measured pulse was 64 s.

Wood

The RTDs for all wood samples are shown in Fig. 15. Both the peak position and magnitude show a good match between FD and TD data for all wood samples. The main peak position for the samples is varying between 0.7 and 20 s.

Sandstone

Fig. 16 displays the RTDs of the sandstone samples. Depending on the TD data quality, RTDs obtained from TD and FD data match well or only moderate. The RTDs for the Röttbacher sample (Fig. 16a) show a good agreement in particular for small relaxation times (<10 s). Higher relaxation times cannot be sufficiently resolved in TD due to the limited pulse lengths (max. 64 s). This restriction can be observed for all samples. However, for the Langenauer (Fig. 16b) and Oberkirchner samples (Fig. 16c) the peak position is very similar for the FD and TD derived RTDs, but the magnitude of the peak differs considerably.

DISCUSSION

In general, the measured IP data of all samples and the test circuit are consistent and reliable, and in agreement with previous SIP investigations (Martin *et al.* 2015; Kruschwitz *et al.* 2020). In FD, we observed that high-frequency data are affected by electromagnetic noise (and possibly by the Maxwell–Wagner polarization) starting from the frequency of 200 Hz. In TD, we were able to measure

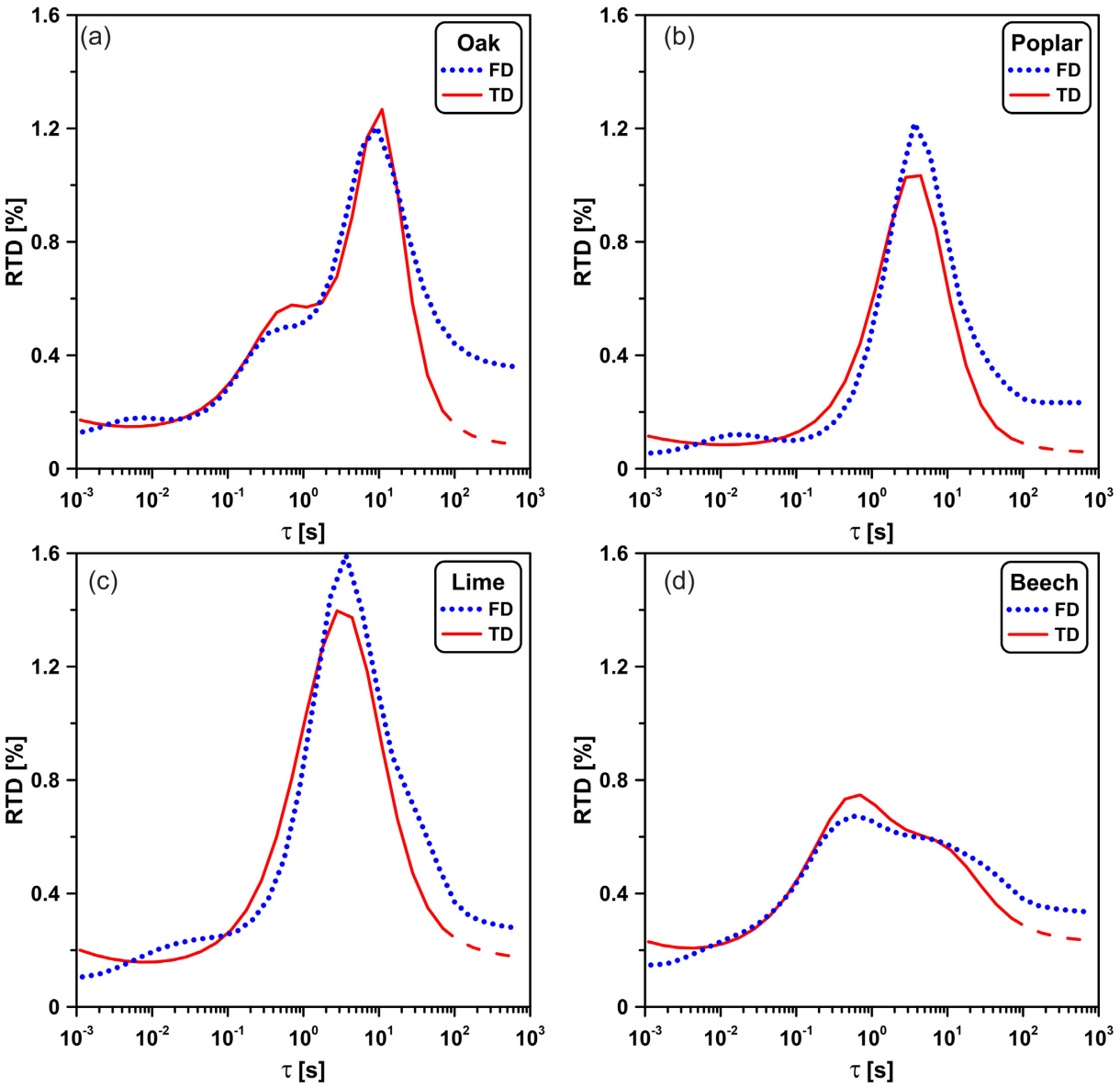

Figure 15. RTD for the wood samples: (a) oak, (b) poplar, (c) lime and (d) beech from FD and TD (1, 8, 64 s) measurements. The dashed line for higher relaxation times in TD represents extrapolated curves because the longest measured pulse was 64 s.

the decays from 0.3 ms until the maximum pulse length of 64 s. The data from the wood samples were not or only slightly affected by noise over the entire TD measurement range. However, some of the sandstone samples (Oberkirchner, Santa Fiora and Baumberger) often show negative decay values at late times (>8 s).

The data quality of the TD measurements depends on the applied current. To avoid an oversteering of the voltage measurement, the selected current output must be adapted to the resistivity of the samples, which results in different currents for the sandstone and wood samples. We applied a current of 100 μA for the wood samples. In contrast, the sandstone samples were measured with a current of only 10 μA. Because of the lower current, the signal-to-noise ratio is reduced compared to the wood samples and the data quality became worse.

The negative decays of some sandstone samples could be caused by electrode polarization effects due to instabilities (in terms of the self-polarization) of the potential electrodes especially for long pulse lengths. If the galvanic coupling is not sufficient, it affects especially the late times or low frequencies (slow processes), and the noise increases with increasing resistivity. Due to the higher resistive sandstone samples, they seem to be more affected by bad coupling. In addition, the higher noise in TD can be attributed to disruptive measurements in the laboratory, which occasionally were running in parallel. In contrast to simple noise suppressing in TD, a more effective digital filtering in FD, which better suppresses the mentioned effects, guarantees a reliable data quality of FD measurements.

The TD decay curves show a dependence of the polarizability from the pulse lengths. This effect is in accordance with eq. (12), where the pulse length strongly influences the magnitude and shape of the decay curve. Also, Mao *et al.* (2016) and Olsson *et al.* (2019) reported similar observation on the influence of the pulse lengths for field TD data.

We observe that the test circuit with only Debye elements ($c = 1$) does not show any differences in the amplitude of the decay curve for varying pulse lengths (Fig. 5b), while the Pelton models with

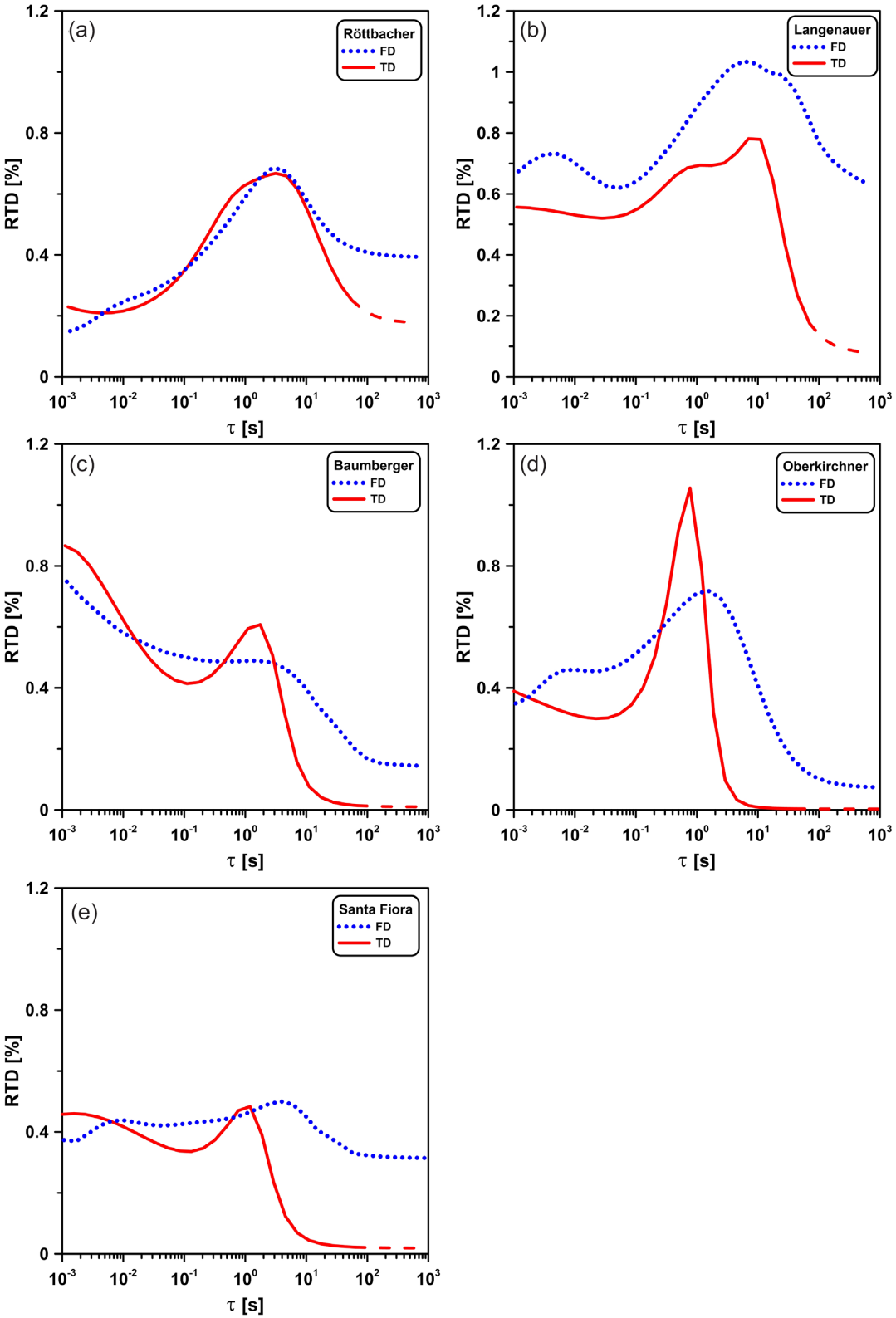

Figure 16. RTD for the sandstone samples: (a) Röttbacher, (b) Langenauer, (c) Baumberger, (d) Oberkirchner and (e) Santa Fiora from FD and TD (1, 8, 64 s) measurements. The dashed line for higher relaxation times in TD represents extrapolated curves because the longest measured pulse was 64 s.

$c < 1$ indicate a remarkable dependence of the decay amplitude on the pulse length. Here, Model 3 with the smallest c-value of 0.3 shows the strongest dependence. This effect can also be observed for the natural samples with small c-values (Table B1 in Appendix B), such as beech ($c = 0.35$, Fig. 8a), Röttbacher ($c = 0.29$, Fig. 10a) and Langenauer ($c = 0.18$, not shown).

The slight differences in the resistivities between FD and TD are also caused by the (finite) pulse lengths (compare Tables A1 and A2

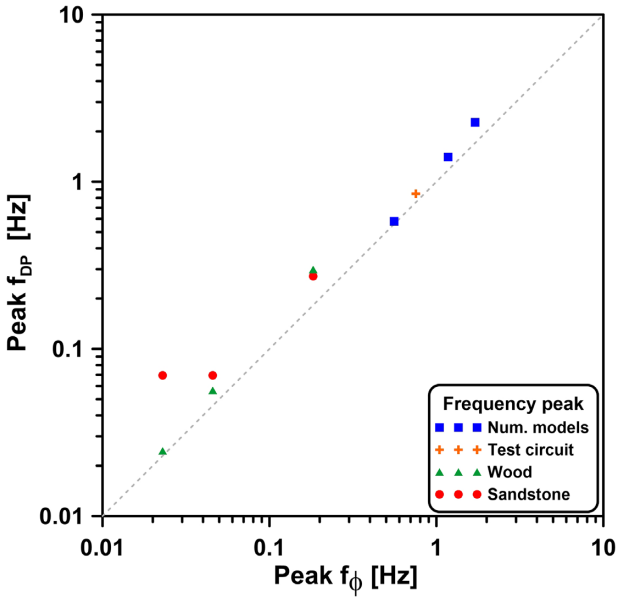

Figure 17. Comparison between the peak frequency for DP and phase.

in Appendix A). In general, the TD resistivity shows an increase with increasing pulse length. Compared with the FD resistivities (@ 0.01 Hz), the TD resistivities are almost always smaller as a result of the short pulse length.

The DP curve is a promising tool to visualize the differences of the decay for various samples, and to compare the TD and FD data at first glance. In contrast to the Debye decomposition procedure, which requires a mathematical solution of an ill-posed problem with a well-chosen regularization, the DP curve results in a straightforward and unique way without any additional constraints. A good agreement between DP and phase could be seen for the test circuit and the numerical models. According to the theory, the relationship between DP and phase depends on the parameters c and m of the Pelton model. For the Debye model ($c = 1$, test circuit), an almost perfect match could be observed, showing a high data similarity, regardless of the pulse lengths. Using the theoretical DP/ ϕ ratio for the Debye model 1 per cent/−13.7 mrad, the DP and phase magnitudes become almost identical, and only the shape of the curve varies. In contrast to the symmetrical phase curve, the DP curve is asymmetric with a steeper slope at lower frequencies or later times.

The numerical models show a comparable behaviour of the DP and phase curves. However, some differences between the pulse lengths are obvious for the low-frequency side because of the missing low-frequency information in TD, even for the 64 s pulse length.

We observe that the two Pelton terms for Model 2 (with a ratio of 10 between the two time constants) and Model 3 (with a ratio of 100 between the time constants) are resolved neither in the phase nor in the DP curves. In contrast to the Model 2 data, where at least a slight hunch for the second peak at $t = 0.05$ s can be seen, the curves of Model 3 do not provide any evidence of two separate relaxation processes. Obviously, the low values of chargeability m and c prevent the formation of separate phase and DP maxima.

For the natural samples, and, in particular, for the wood samples, a very good similarity between DP and phase curves in terms of peak frequency and polarization magnitude can be found. The sandstone samples show some similarities, but not to the same extent as the wood samples. Again, small shifts in magnitude and in frequency can be observed. In addition to the non-Debye behaviour of the data, their quality in TD seems to affect the comparability. We found that a better data quality improves the similarity between DP and phase curves.

To compare the measured data, a correlation between the peak frequencies for both DP and phase curves is shown in Fig. 17. The deviations for the peak frequencies are very low and shifted approximately 10 per cent to higher frequencies for DP. This deviation is also caused by the non-Debye behaviour of most of the samples and a result of eq. (12) (see also Titov *et al.* 2002).

To compare the TD and FD data in more detail, both data sets were transformed to RTDs based on the Debye decomposition approach. For that comparison, we used the TD data from three different pulse lengths to get a better resolution over the entire bandwidth (e.g. 1, 8, 64 s) according to Tarasov & Titov (2007). The RTDs for the test circuit and the three numerical models match excellent.

For the test circuit (Fig. 14a, $\tau = 0.22$ s), Model 1 (Fig. 14c, $\tau = 0.1$ s) and Model 2 (Fig. 14b, $\tau_1 = 0.05$ s and $\tau_2 = 0.5$ s), the expected initial parameters are well recovered (Fig. 14, Tables 1 and 2). For Model 3, the different time constants cannot be resolved ($\tau_1 = 0.05$ s and $\tau_2 = 5$ s). Even though the time constants are separated by a factor of 100 (instead of a factor of 10 in Model 2), the small c-value hinders a separation in the RTD. Instead, one broad maximum at around $\tau = 0.1$ s is observed.

Depending on the data quality, the RTDs obtained from FD and TD data are in a very good to moderate agreement. In Fig. 18, a comparison between the TD and FD RTD parameters, the τ value for the main peak (a) and the peak magnitude (b) are shown. In order to compare the deviation quantitatively, we calculated an average absolute deviation as presented in Weller *et al.* (2015, eq. 18), where a deviation of $d = 1$ denotes an average absolute deviation of one order of magnitude (or a factor of 10).

As can be seen for the test circuit and the numerical models, the RTD parameters for both domains are very similar and, therefore, only with small deviations ($d = 0.03$ and 0.004, respectively).

The results for the wood samples (green triangles) are also in good agreement. The deviations for the relaxation times (Fig. 18a) are a bit higher ($d = 0.09$) than those for the RTD magnitudes (Fig. 18b, $d = 0.05$).

The RTD data for the sandstone samples (red circles), obtained from TD and FD measurements, are in general agreement. However, due to the moderate data quality for late times in TD (which is related to very small voltage values), the RTDs could not always be calculated as exactly as in FD, and discrepancies in terms of the magnitude ($d = 0.28$) and time/frequency shifts ($d = 0.08$) appeared.

According to our findings, we can summarize the following: First, the RTD is very useful to compare TD and FD data. This enables the possibility to conduct accurate and time-consuming FD IP measurements in the laboratory and to compare them qualitatively with TD IP field measurements. Second, differences in the RTD between TD and FD are mainly produced by the raw data quality in TD. Therefore, good data quality should be ensured as much as possible in any case.

CONCLUSIONS

IP data measured in TD or FD provide similar information. The results from all samples as well as from the numerical models

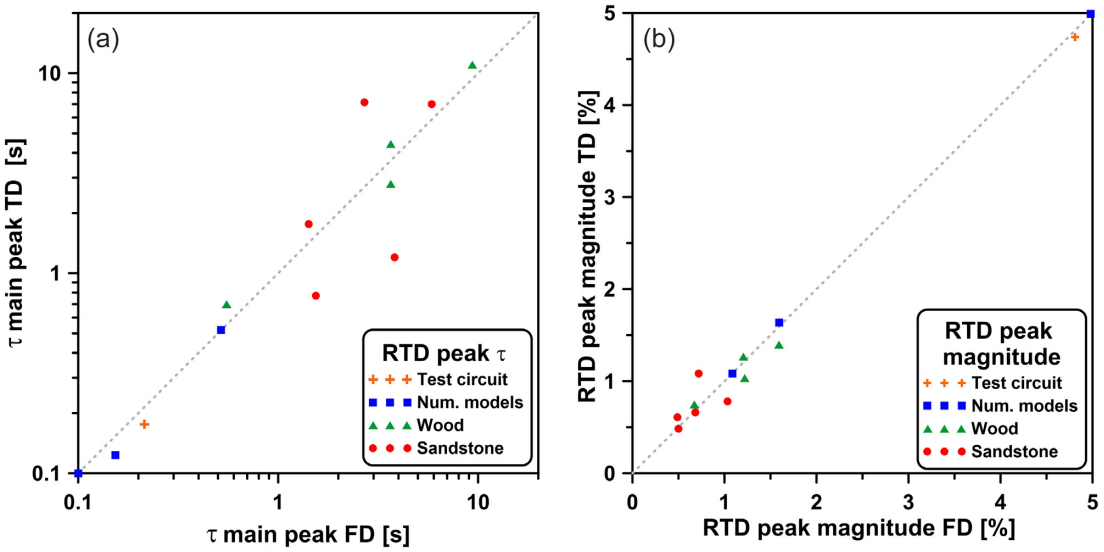

Figure 18. Comparison of RTDs in TD and FD: (a) relaxation time τ for the main peak; (b) RTD magnitude for the main peak.

and the test circuit reveal a good comparability for laboratory IP measurements in both TD and FD. Insufficient raw data quality has the strongest effect on the comparability between FD and TD. In particular, measurements in TD are more affected by noise, for example, due to the electrode polarization. In turn, measurements in FD can resolve better low-frequency signals because of the applied digital filtering. Therefore, it is highly recommended to use non-polarizable electrodes, in particular for TD measurements.

The concept of DP has proved to be a suitable transformation of TD decays that enables an easier visual discrimination between different samples and a good comparison to the phase spectra resulting from FD measurements. It has been shown that both DP and phase curve contain similar information. This enables a fast and direct matching of the measured raw IP data.

Furthermore, the RTD was successfully used to transform the data from both domains, and often a high similarity between TD and FD RTDs is obtained.

In summary, depending on the aimed IP information, IP laboratory measurements can result in comparable spectral results in both TD and FD. Nevertheless, considering the data quality especially at the low-frequency range, measurements in FD might be favoured in the laboratory environment. The transformation of IP spectra acquired in the laboratory to RTDs enables a comparison with the RTDs of the TD decay curves measured in the field.

ACKNOWLEDGEMENTS

This project has received funding from the European Union's Horizon 2020 Framework Programme under the Marie Sklodowska-Curie Grant Agreement No. 752671. TM thanks Sabine Kruschwitz (BAM Berlin) for providing and helping with the natural samples. Furthermore, the authors thank Brahim Mehalli, Viacheslav Emelianov, Elvina Ikhina and Gregory Gurin for the support in the laboratory of St Petersburg State University. KT and AT acknowledge the support of Russian Science Foundation through Grant No. 20-47-04402. AW acknowledges the support of DFG through Grant No. WE 1557/17-1. Equipment of RC "Geomodel" Core Facility of St Petersburg State University was used. We also appreciate the work of the two reviewers (L. Levy and anonymous) whose comments have significantly improved the manuscript.

DATA AVAILABILITY

The data discussed in this paper are available upon request.

REFERENCES

Binley, A., Slater, L.D., Fukes, M. & Cassiani, G., 2005. Relationship between spectral induced polarization and hydraulic properties of saturated and unsaturated sandstone, *Water Resour. Res.,* **41,** W12417, doi:10.1029/2005WR004202.

Börner, F.D. & Schön, J.H., 1991. A relation between the quadrature component of electrical conductivity and the specific surface area of sedimentary rocks, *Log Analyst,* **32,** 612–613.

Cole, K.S. & Cole, R.H., 1941. Dispersion and adsorption in dielectrics. I. Alternating current characteristics, *J. Chem. Phys.,* **9,** 341–351.

Debye, P., 1929. *Polar Molecules,* Chemical Catalog Co., Inc., 172pp.

Fiandaca, G., Ramm, J., Binley, A., Gazoty, A., Christiansen, A.V. & Auken, E., 2013. Resolving spectral information from time domain induced polarization data through 2-D inversion, *Geophys. J. Int.,* **192**(2), 631–646.

Flores Orozco, A., Kemna, A., Oberdorster, C., Zschornack, L., Leven, C., Dietrich, P. & Weiss, H., 2012. Delineation of subsurface hydrocarbon contamination at a former hydrogenation plant using spectral induced polarization imaging, *J. Contam. Hydrol.,* **136–137,** 131–144.

Gurin, G., Tarasov, A., Ilyin, Y. & Titov, T., 2013. Time domain spectral induced polarization of disseminated electronic conductors: laboratory data analysis through the Debye decomposition approach, *J. Appl. Geophys.,* **98,** 44–53.

Gurin, G., Titov, K., Ilyin, Y. & Tarasov, A., 2015. Induced polarization of disseminated electronically conductive minerals: a semi-empirical model, *Geophys. J. Int.,* **200**(3), 1555–1565.

Johansson, S., Lindskog, A., Fiandaca, G. & Dahlin, T., 2020. Spectral induced polarization of limestones: time domain field data, frequency domain laboratory data and physicochemical rock properties, *Geophys. J. Int.,* **220**(2), 928–950.

Kemna, A., 2000. Tomographic inversion of complex resistivity—theory and application, *PhD thesis*, Ruhr-University Bochum, Germany.

Kemna, A. *et al.*, 2012. An overview of the spectral induced polarization method for near-surface applications, *Near Surf. Geophys.,* **10,** 453–468.

Kessouri, P. *et al.*, 2019. Induced polarization applied to biogeophysics: recent advances and future prospects, *Near Surf. Geophys.,* **17,** 595–621.

Komarov, V.A., 1980. *Electrorazvedka Metodom Vyzvannoi Polarizatsii (Electrical Prospecting Using Induced Polarization Method),* Nedra Press (in Russian).

Kruschwitz, S., 2007. Assessment of the complex resistivity behavior of salt affected building materials, *PhD thesis*, TU Berlin, Germany.

Kruschwitz, S., Halisch, M., Dlugosch, R. & Prinz, C., 2020. Toward a better understanding of low-frequency electrical relaxation—an enhanced pore space characterization, *Geophysics,* **85,** MR257–MR270.

Madsen, L.M., Fiandaca, G., Auken, E. & Christiansen, A.V., 2017. Time-domain induced polarization—an analysis of Cole–Cole parameter resolution and correlation using Markov Chain Monte Carlo inversion, *Geophys. J. Int.,* **211**(3), 1341–1353

Mao, D., Revil, A. & Hinton, J., 2016. Induced polarization response of porous media with metallic particles—part 4: detection of metallic and nonmetallic targets in time-domain induced polarization tomography, *Geophysics,* **81**(4), D359–D375.

Martin, T., 2012. Complex resistivity measurements on oak, *Eur. J. Wood Wood Prod.,* **70,** 45–53.

Martin, T., Nordsiek, S. & Weller, A., 2015. Low-frequency impedance spectroscopy of wood, *J. Res. Spectrosc.,* **2015**(2015), Article ID 910447.

Martin, T., Günther, T., Flores Orozco, A. & Dahlin, T., 2020. Evaluation of spectral induced polarization field measurements in time and frequency domain, *J. Appl. Geophys.,* **180,** doi:10.1016/j.jappgeo.2020.104141.

Maurya, P.K., Fiandaca, G., Christiansen, A.V. & Auken, E., 2018. Field-scale comparison of frequency- and time-domain spectral induced polarization, *Geophys. J. Int.,* **214,** 1441–1466.

Nordsiek, S. & Weller, A., 2008. A new approach to fitting induced-polarization spectra, *Geophysics,* **73**(6), 235–245.

Olsson, P.-I., Fiandaca, G., Maurya, P.K., Dahlin, T. & Auken, E., 2019, Effect of current pulse duration in recovering quantitative induced polarization models from time-domain full-response and integral chargeability data, *Geophys. J. Int.,* **218**(3), 1739–1747.

Ontash & Ermac, 2018, *O & E Portable Spectral Induced Polarization (SIP) Field/Lab Unit (PSIP) User Guide,* Ontash & Ermac, Inc, http://www.ontash.com.

Pelton, W.H., Ward, S.H., Hallof, P.G., Sill, W.R. & Nelson, P.H., 1978. Mineral discrimination and removal of inductive coupling with multifrequency IP, *Geophysics,* **43,** 588–609.

Radic Research, 2019. SIP Fuchs III+ user manual. http://www.radic-research.de/Flyer_SIP-Fuchs-III+_240119.pdf.

Schlumberger, C., 1920. *Etude sur la Prospection ÉLectrique du Soussol,* Gauthier-Villars, Chap. VIII.

Seigel, H., Nabighian, M., Parasnis, D.S. & Vozoff, K., 2007. The early history of the induced polarization method, *Leading Edge,* **26**(3), 312–321

Tarasov, A. & Titov, K., 2007. Relaxation time distribution from time domain induced polarization measurements, *Geophys. J. Int.,* **170,** 31–43.

Tarasov, A. & Titov, K., 2013. On the use of the Cole–Cole equations in spectral induced polarization, *Geophys. J. Int.,* **195**(1), 352–356.

Tikhonov, A.N. & Arsenin, V.Y., 1977. *Solution of Ill-posed Problems,* Winston & Sons.

Titov, K., Komarov, V., Tarasov, A. & Levitsk, A., 2002. Theoretical and experimental study of time domain-induced polarization in water-saturated sands, *J. Appl. Geophys.,* **50**(4), 417–433.

Vanhala, H. & Soininen, H., 1995. Laboratory technique for measurement of spectral induced polarization response of soil samples, *Geophys. Prospect.,* **43,** 655–676.

Weigand, M. & Kemna, A., 2016. Debye decomposition of time-lapse spectral induced polarisation data, *Comput. Geosci.,* **86,** 34–45

Weller, A. & Börner, F., 1996. Measurements of spectral induced polarization for environmental purposes, *Environ. Geol.,* **27,** 329–334.

Weller, A., Slater, L., Binley, A., Nordsiek, S. & Xu, S., 2015. Permeability prediction based on induced polarization: insights from measurements on sandstone and unconsolidated samples spanning a wide permeability range, *Geophysics,* **80**(2), D161–D173.

Wong, J., 1979. An electrochemical model of the induced-polarization phenomenon in disseminated sulfides ores, *Geophysics,* **44**(7), 1245–1265.

Zhang, Z., Kruschwitz, S., Weller, A. & Halisch, M., 2018. Enhanced pore space analysis by use of μ-CT, MIP, NMR, and SIP, *Solid Earth,* **9,** 1225–1238.

Zimmermann, E., 2010. Phasengenaue Impedanzspektroskopie und -tomographie für geophysikalische Anwendungen (Phase-accurate impedance spectroscopy and tomography for geophysical applications, *PhD thesis*, University Bonn, Germany.

Zonge, K., Sauck, W. & Sumner, J., 1972. Comparison of time, frequency, and phase measurements in induced polarization, *Geophys. Prospect.,* **20,** 626–648.

APPENDIX A: MEASUREMENT SETTINGS AND RESULTS FOR THE WOOD AND SANDSTONE SAMPLES

Table A1 provides the settings for the TD measurements for the wood samples and Table A2 for the sandstone samples. The calculated resistivity value can be compared with the FD resistivity at the frequency $f = 0.01$ Hz. As mentioned in the discussion, the slight differences in the resistivities between FD and TD are caused by the (finite) pulse lengths. In general, the TD resistivity shows an increase with increasing pulse length. Compared with the FD resistivities (@ 0.01 Hz), the TD resistivities are almost always smaller because of the short pulse length.

APPENDIX B: INFLUENCE OF THE *c* PARAMETER ON THE COMPARISON BETWEEN DP AND PHASE CURVES

Based on the measured data, an empirical relationship between DP and phase magnitude can also be obtained. Fig. B1 shows the measured values together with the theoretical curves for $c = 1$ and $c = 0.5$ for different m (see also Fig. 1). The single data point of the test circuit shows a very good agreement with the predicted theoretical values for $c = 1$ due to the Debye behaviour of the test circuit. However, the data points from the Pelton models and the natural samples follow a curve with a smaller slope that corresponds more or less to a Pelton model with $c = 0.5$ and a DP/ ϕ ratio = 1 per cent/−16.6 mrad. Regarding Fig. 1 and B1, the dependence of the DP/ ϕ ratio on c and m becomes obvious.

In theory, the polarization magnitude depends also on the parameter c of the Pelton model (eq. 19). Therefore, we conducted a fitting to receive the respective parameters of the Pelton model for our models and suitable samples with a clear maximum in the phase spectrum. The resulting values are compiled in Table B1. The theoretical dependence of the ratio DP/ ϕ on c and m is demonstrated in Fig. B2. We observe for higher values of c a smaller DP/ ϕ ratio. The data points of the wood samples confirm this relationship. In contrast, some of the sandstone samples show higher deviation (outliers with too high ratios: Langenauer and Oberkirchner), most likely due to the modest data quality of the TD measurements. Only the data point of the Röttbacher sample shows the expected ratio. Therefore, an estimation of the c-value from the relationship between the FD phase and TD DP data seems to be possible only if a sufficient data quality can be achieved.

APPENDIX C: MEASURABLE POLARIZATION DECAY AFTER A SERIES OF CURRENT PULSES

When current pulses of opposite polarity are used to excite IP in TD, the full current waveform (pulse and pause durations) can strongly

Table A1. TD measurement settings and results for the four wood samples together with the FD resistivity value for $f = 0.01$ Hz.

Sample	TD pulse length (s) / stacks	1 / 10	2 / 10	4 / 10	8 / 8	16 / 6	64 / 4	FD @ 0.01 Hz
Oak	I (μA)	100	100	100	100	100	100	142
	U (mV)	509	515	521	529	536	546	810
	ρ (Ωm)	40.1	40.5	41.1	41.7	42.2	43	45
Poplar	I (μA)	100	100	100	100	100	100	276
	U (mV)	220	222	225	228	231	233	709
	ρ (Ωm)	17.7	17.9	18.2	18.4	18.7	18.9	20.3
Lime	I (μA)	100	100	100	100	100	100	183
	U (mV)	396	403	411	418	423	430	917
	ρ (Ωm)	31.2	31.8	32.4	32.9	33.3	33.9	39.4
Beech	I (μA)	100	100	100	100	100	100	178
	U (mV)	536	542	548	553	559	568	968
	ρ (Ωm)	42.2	42.7	43.2	43.6	44.1	44.8	42.9

Table A2. TD measurement settings and results for the five sandstone samples together with the FD resistivity value for $f = 0.01$ Hz.

Sample	TD pulse length (s) / stacks	1 / 10	2 / 10	4 / 10	8 / 8	16 / 6	64 / 4	FD @ 0.01 Hz
Rött	I (μA)	10	10	10	10	10	10	37
	U (mV)	220	222	225	227	228	231	882
	ρ (Ωm)	135	136	138	139	140	142	145
SF	I (μA)	10	10	10	10	10	10	34
	U (mV)	210	211	212	213	214	213	745
	ρ (Ωm)	129	130	130	131	131	131	136
OK	I (μA)	10	10	10	10	10	10	31
	U (mV)	269	270	270	273	273	274	948
	ρ (Ωm)	165	166	166	168	168	168	184
Baum	I (μA)	10	10	10	10	10	10	48
	U (mV)	113	114	115	112	117	118	575
	ρ (Ωm)	69.4	70	70.6	68.8	71.8	72.4	73
Lang	I (μA)	10	10	10	10	10	10	58
	U (mV)	158	160	162	163	165	168	1006
	ρ (Ωm)	125	126	128	128	130	132	136

influence the magnitude and shape of IP decays, which depend on the pulse length and the characteristic relaxation time.

A series of opposite current pulses with pause between them can be expressed by a combination of the shifted step functions:

$$I(t) = I_o \cdot \sum_{k=0}^{N} (-1)^k (\gamma(t - 2kT) - \gamma(t - (2k+1)T), \qquad \text{(C1)}$$

where I_o is the current magnitude, $\gamma(t)$ is the step function [$\gamma(t) = 1$ for $t < 0$ and $\gamma(t) = 0$ for $t > 0$], T is the duration of the current pulses and pauses and N is the number of the pulses.

In this case, the measured polarizability decay $\widehat{\eta}(t, T)$ after a series of current pulses can be written as

$$\widehat{\eta}(t, T) = \sum_{k=0}^{N} (-1)^k [\eta(t + 2kT) - \eta(t + (2k+1)T)]. \qquad \text{(C2)}$$

If $\eta(t)$ is a simple Debye decay (eq. 8), then eq. (C2) can be rewritten as

$$\widehat{\eta}(t, T) = m \sum_{k=0}^{N} (-1)^k [\exp((t + 2kT)/\tau) - \exp((t + (2k+1)T)/\tau)]. \qquad \text{(C3)}$$

For $\rightarrow \infty$, eq. (C2) has the following limit:

$$\widehat{\eta}(t, T) = m \cdot \exp(-t/\tau)[(1 - \exp(-T/\tau)) \times \frac{1 - \exp(-2T/\tau) + \exp(-4T/\tau)}{1 - \exp(-4T/\tau)}]. \qquad \text{(C4)}$$

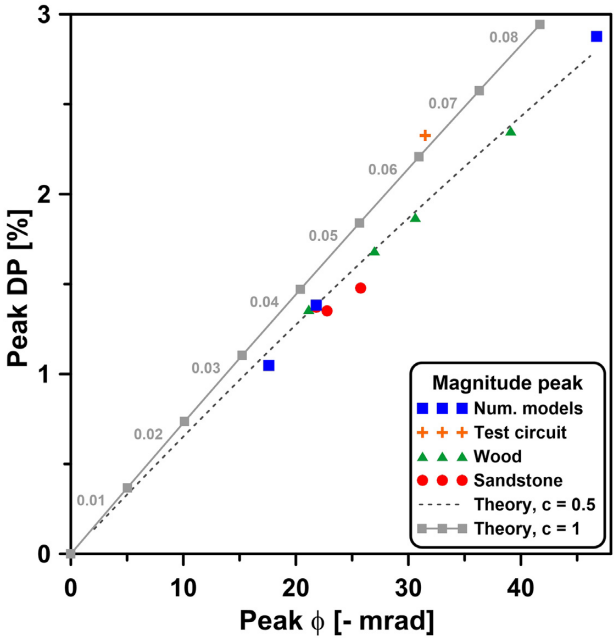

Figure B1. Comparison between the peak magnitude for DP and phase for both the measured data (coloured) and the theoretical calculated values for different m values for a Debye model (grey, compare also Fig. 1) and the Pelton model (with $c = 0.5$, dashed line).

Table B1. Parameters for all models and samples with a Pelton behaviour.

Sample	ρ_{DC} (Ωm)	m (-)	τ (s)	c (-)
Test circuit	163.5	0.062	0.22	0.98
Model 1	100	0.100	0.10	0.50
Model 2	100.3	0.153	0.25	0.67
Model 3	99.9	0.154	0.16	0.26
Oak	47.9	0.144	7.62	0.44
Poplar	20.8	0.093	4.98	0.62
Lime	41.2	0.148	4.37	0.55
Beech	44.9	0.139	1.97	0.35
Roett	156	0.173	6.37	0.29
OK	189	0.128	0.37	0.40
Lan	160	0.131	29	0.18

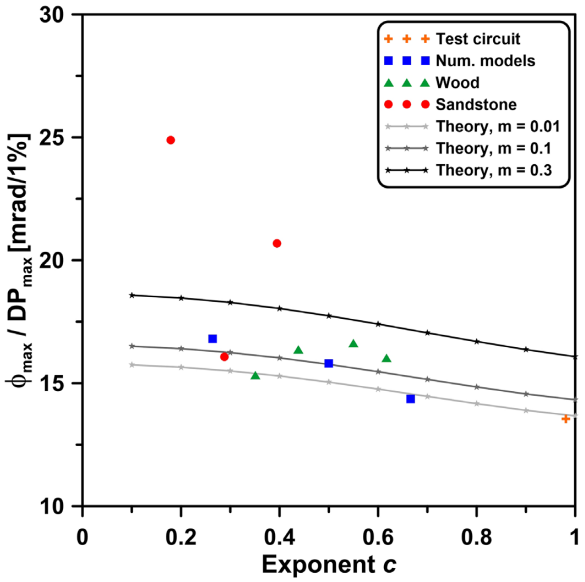

Figure B2. Relationship between the DP/ϕ ratio and c from the theory with varying m (grey lines), the test circuit, the numerical models and the measured samples.